Chemosphere 303 (2022) 134955

Contents lists available at ScienceDirect

Chemosphere

journal homepage: www.elsevier.com/locate/chemosphere

Arsenic contamination at the Bagnoli Bay seabed (South Italy) via particle tracking numerical modeling: Pollution patterns from stationary climatic forcings

Mariano Buccino [a,*], Mohammad Daliri [a], MS. Norma Buttarazzi [a], Giuseppe Del Giudice [a], Mario Calabrese [a], Renato Somma [b,c]

[a] Department of Civil, Architectural and Environmental Engineering, University of Napoli, Federico II. Via Claudio 21, 80125, Napoli, Italy
[b] INGV. Osservatorio Vesuviano, Via Diocleziano, 324-80124, Napoli, Italy
[c] IRISS CNR, Via G. Sanfelice, 8, 80134, Napoli, Italy

HIGHLIGHTS

- We used a particle tracking numerical model to assess the impact of an artificial drain on arsenic contamination of marine sediments in Bagnoli bay (South Italy).
- We measured the flow rate of the drain between February and June 2021.
- We used climate forcings including tides, wind and waves.
- We compared numerical contamination patterns to measurements carried out within the research project ABBaCo.
- We found out tidal circulation is the leading driver of the contamination process.

GRAPHICAL ABSTRACT

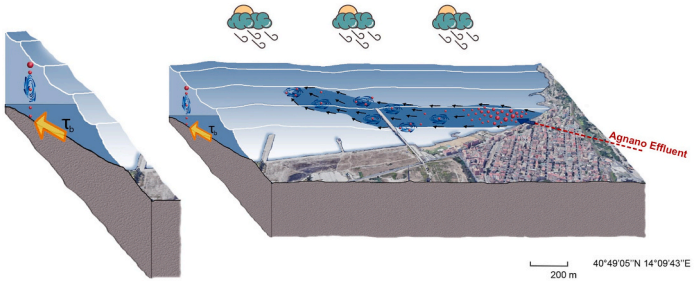

ARTICLE INFO

Handling Editor: Derek Muir

Keywords:
Arsenic contamination in marine sediments
Numerical modeling
Diffusion in coastal waters
Particle tracking
Sediments settling
Adsorption

ABSTRACT

Almost 140 years of industrial exploitation have severely degraded the environment of Bagnoli Coroglio (BC), the westernmost neighborhood of the city of Naples (Italy). In this peculiar area, however, geogenic processes overlap with the impact of human activities, making it difficult to distinguish between anthropogenic and geogenic pollution sources. This is particularly true for Arsenic, the concentration of which in the marine sediments largely exceeds the tolerable level for human health and the background value for local pyroclastics.

After several studies have used traditional tools based on multivariate statistics, this article attempts at tackling the problem via numerical modeling, which provides a deeper insight into the physics that governs the pollution process.

Therefore, we use a particle tracking model to assess whether arsenic levels in the seabed can be affected by the influx of thermal water from an artificial channel outfalling at the westernmost part of the coast The climatic forcings that drive the marine circulation are simplified to basic "scenarios", in which wind and waves are stationary in strength and direction. Since the simulation time is much less than the contamination timescale, the comparison between numerical results and measurements is essentially qualitative and concerns the shape of contamination contours.

* Corresponding author.
E-mail address: buccino@unina.it (M. Buccino).

https://doi.org/10.1016/j.chemosphere.2022.134955
Received 4 March 2022; Received in revised form 4 May 2022; Accepted 10 May 2022
Available online 22 May 2022

It was found the primary forcing that enables seabed pollution is the tidal circulation, which, moreover, acts continuously in time.

Quantitative arguments based on regression analysis suggest the discharge of thermal water explains almost a quarter of the observed pollution, which is consistent with previous research based on multivariate statistics.

1. Introduction

Bagnoli-Coroglio (BC) is the westernmost district of the city of Naples (southern Italy) and is part of the Campi Flegrei caldera (CFc), one of the most explosive volcanic areas in Europe. It overlooks the Tyrrhenian Sea for about 3 km and is featured with a bay-shaped coastline completely Enclosed by the Gulf of Pozzuoli (Fig. 1).

For almost 140 years (1854–1992), BC experienced intense industrialization and was home to the second-largest integrated steel plant in Italy (ILVA-ITALSIDER) as well as factories producing asbestos, cement, and fertilizers. In the mid-20th century, ILVA's processing needs required the construction of four piers and a wide platform made of concrete and blast furnace slag (Fig. 2).

When all industrial activities finally ceased, the Italian government drew up a rehabilitation plan to restore the area's original beauty and tourist appeal. This, of course, demands intensive remediation measures, as industrial exploitation has dramatically impacted the inland and coastal environment, including marine sediments (ICRAM-SZN, 2005; Romano et al., 2009, 2018; Trifuoggi et al., 2017; Armiento et al., 2020; Passaretti et al., 2020; Tamburrino et al., 2020).

Among the contaminants of the seabed (organic compounds, heavy metals/metalloids), arsenic (As) is particularly noteworthy, as highlighted in several recent studies (among the others, Chen et al., 2017; Liu et al., 2022, Haghnazar et al., 2021).

Fig. 3 shows the concentration in the first meter of sediment is in the order of 100 mg/kg (Fig. 3), which is far above the tolerable level for human health and exceeds the background for CFc pyroclastics by a factor of 10 (Damiani et al., 1987).

The peculiarity of arsenic lies in its uncertain origin. The limited correlation with organic compounds indicates the simultaneous influence of anthropogenic activities and geogenic processes related to the volcanic character of BC. Other pollutants such as chromium, nickel and vanadium behave similarly, but none of them exhibit a clear correlation with arsenic (Armiento et al., 2020).

Recent research studies based on multivariate statistics (Giglioli et al., 2020; Somma et al., 2021) suggest that geogenic contamination sources such as submarine fumaroles and thermal springs, likely play a minor role in the process. Giglioli et al. (2020) focused on the 13 thermal springs originally examined by Albanese et al. (2010), and found a negligible correlation (less than 0.1) with arsenic pollution in 6 cases. Similarly, Somma et al. (2021), concluded the position of submarine fumaroles does not affect the contamination pattern.

Conversely, those investigations indicate that a realistic mechanism

Fig. 2. ILVA's platform ("colmata") and piers.

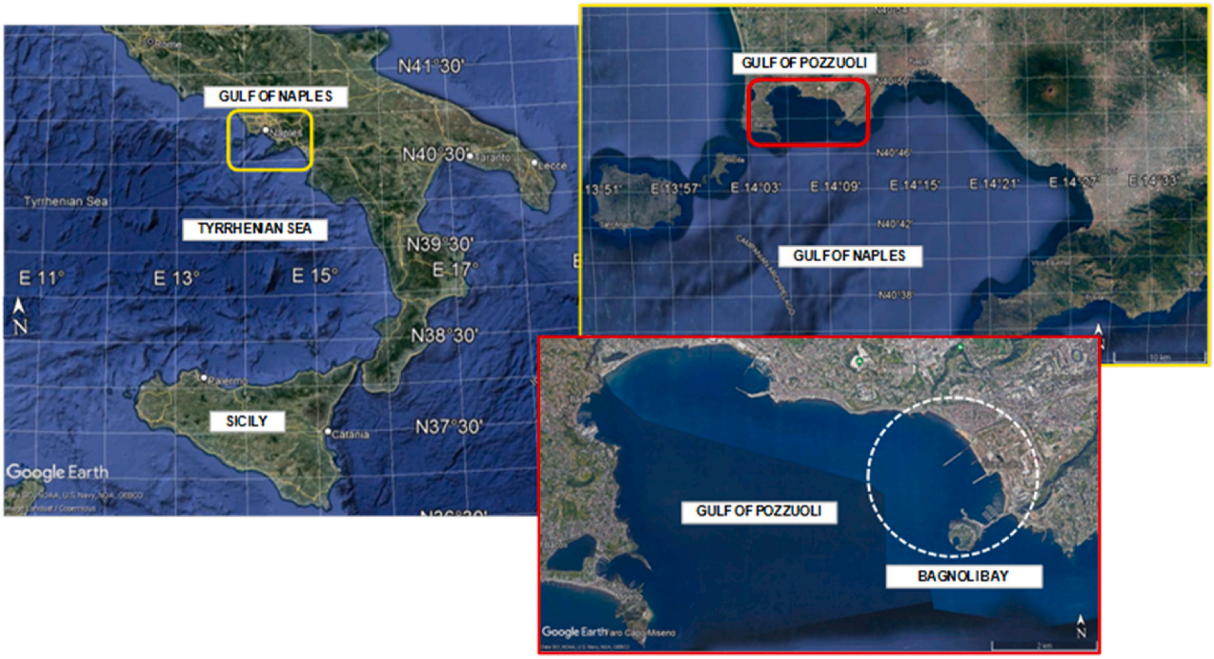

Fig. 1. Location of the Bagnoli bay.

could be the inflow of As-enriched water from inland, especially from the northwestern side of the bay. For this reason, we are drawing particular attention to the "Agnano Effluent" (AE) outlined in Fig. 3, which is the sole outfall still in operation, and could jeopardize future remediation measures.

Since 1865, AE has been conveying a mixture of arsenical groundwater and rainwater from the nearby Agnano area. Because of the abundance of groundwater, the influx into the sea is rather continuous, as suggested by ten flow rate measurements taken over expressly for this research in the period 2021/02/18–2021/06/07 (Fig. 4). By applying a simple linear reservoir model to the data (Maillet, 1905) we infer a "mean residence time" of 53 days (dotted curves in Fig. 4) implying the flow rate at the mouth vanishes only after 165 consecutive dry days.

A numerical investigation carried out by the authors using the Delft3D software package (Buccino et al., 2021) shows the marine circulation of the Bagnoli bay favors the transport of the water discharged by the Agnano Effluent towards the ILVA's piers, which provides indirect evidence of the potential impact of this outfall.

In the sections below, flow rate data and results of marine current analysis form the input of a particle tracking numerical model (Delft3D-PART), which simulates the effects of advection, dispersion and settling on the released arsenic. Delft3D- PART enables to reconstruct the pollution contours on the seabed, and compare them with the measurements.

Despite the comparison being essentially qualitative, mainly due to the process time-scale, it sheds some light on the climatic and hydrographic conditions that control the contamination.

Although relating to a specific site, the approach employed is novel and general, and can provide physical support to traditional tools based on multivariate statistics. This corroborates the argument by Samaras et al. (2016) that numerical modeling has become an essential component of today's coastal planning, decision support and risk assessment, even for highly complex phenomena (Archetti and Lamberti, 2003; Larsen and Fuhrman, 2019; Buccino et al., 2019a, 2019b).

The article is structured as follows. Section 2 summarizes the main characteristics of the Bagnoli bay hydrodynamics, introduces Delft3D-PART, and discusses the related simulation parameters. Numerical pollution patterns are compared with measurements in Section 3, while Section 4 discusses the obtained results. Finally, conclusions are drawn in Section 5.

2. Materials and methods

2.1. Bagnoli bay hydrodynamics from quasi-stationary climatic forcings

Buccino et al. (2021) studied the flow regime of Bagnoli Bay using two modules of the software package Delft3D, namely Delft3D-WAVE for the propagation of short waves and Delft3D- FLOW, to solve the Reynolds-averaged Navier-Stokes equations. The study is somehow similar to that carried out by Gaeta et al. (2020) for other sites in South Italy.

A grid sensitivity study based on a single tide constituent led to discretizing the computational volume (0.045 km^3) into 279 cells in the horizontal plane, and eight layers in the vertical direction. Further reduction in the cell sizes was observed to give a maximum error of 4.8% on the signal's standard deviation and 1.3% on the mean.

To facilitate interpretation of the results, nine " *climatic scenarios*" (CS) were created, in which wind and waves are stationary in direction and magnitude. All the scenarios include the effects of tide, which are accounted for by superimposing five sinusoidal constituents (3 semi-diurnal and 2 diurnal).

The CSs are summarized in Table 1; the letter "M" indicates that wind and waves originate from the respective modal directional sectors, while the acronym "SE" refers to the rare but relatively intense attacks from the southeast. Note that, unlike the waves, the wind climate is characterized by 2 modal directions, one from NE (slightly prevailing in winter), the other from S-SW (prevailing in summer). Finally, the scenario "T-O" has no forcings other than the tide ("Tide Only").

It could be noticed that the direction of wave attacks in Table 1 is almost identical to that considered in Giglioli et al. (2020), based on a 40 years data series from the WAM model. The authors used a wave height of 0.93 m, about halfway between M-4 and M-6, and a period of 4.3s, which gives waves considerably steeper than in Table 1. As will be shown later, however, wave period can be considered a secondary variable in the process under study.

The analysis of the flow field (Fig. 5) revealed that the circulation in the bay is predominantly anticyclonic, which is consistent with the transport of pollutants from the AE mouth towards the piers. The circulation shape is in agreement with the measurements conducted by Castagno et al. (2020), against which the hydrodynamic model was validated.

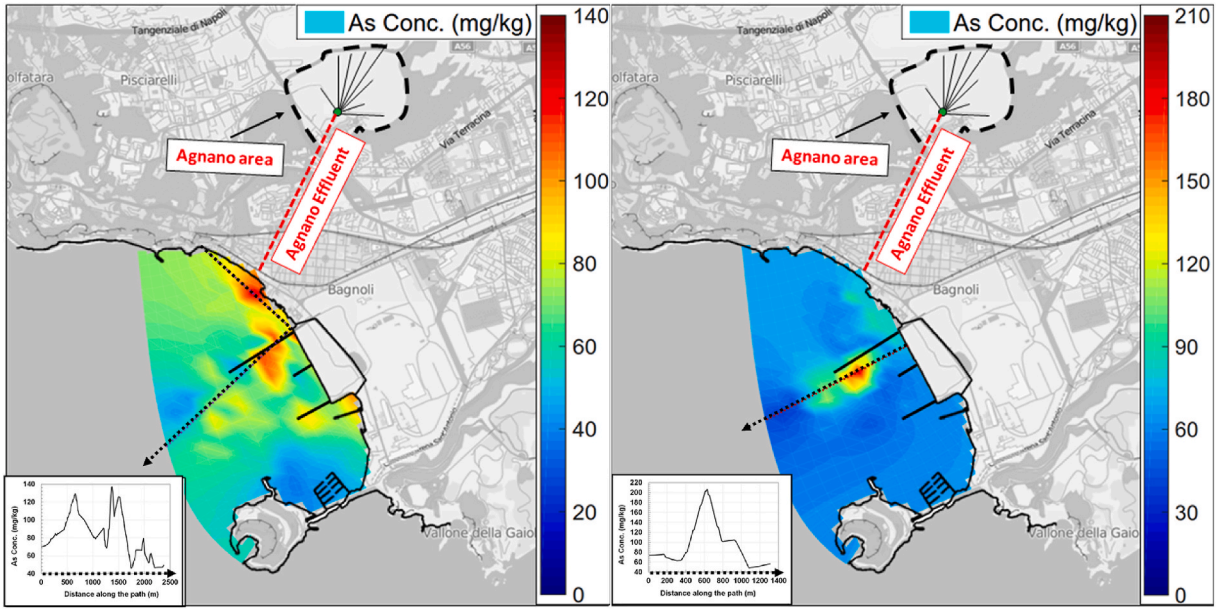

Fig. 3. Arsenic concentration at the Bagnoli bay seabed (ABBaCo project survey). Left panel: upper layer of marine sediments (0-50 cm). Right panel: 50 cm-100cm. Low side panels show concentration along the black dotted path.

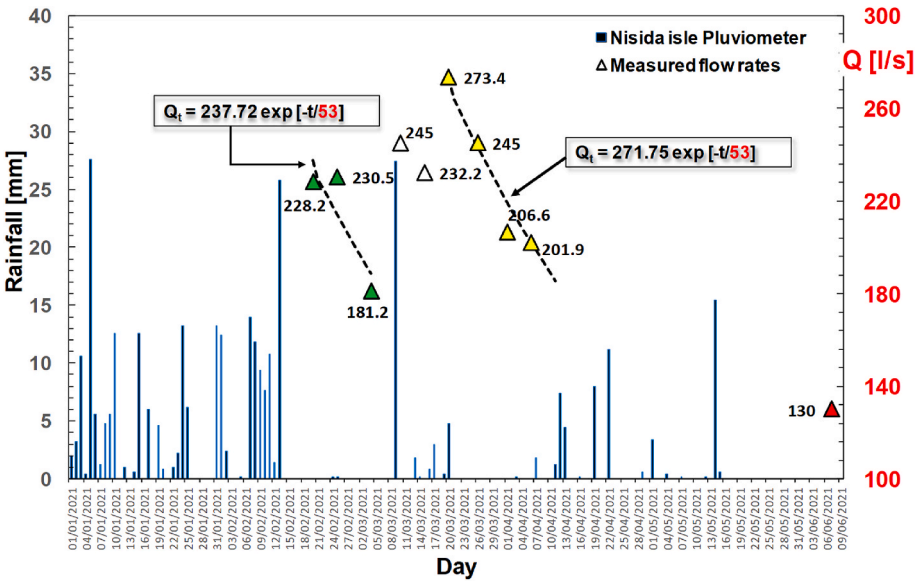

Fig. 4. AE flow rates measurements taken in dry days via float method (triangles). Blue bins represent rainfall detected at the Bagnoli Bay (Nisida ile's pluviometer). In the "recession curves" (dotted lines), Q_t represents the discharge after "t" consecutive dry days. (For interpretation of the references to colour in this figure legend, the reader is referred to the Web version of this article.)

Table 1
Summary of CSs. Bold numbers in parentheses represent percentiles based on conditional distribution functions presented by Buccino et al. (2021). (*) Scenario used in this article for the first time.

CS	Description	Wind direction [°N]	Wind speed [m/s]	Wave direction [°N]	Wave Height [m]	Wave period [s]
T-O	Tide only	–	–	–	–	–
M-1	Tide + Wind	34	2.1 **(50th)**	–	–	–
M-2	Tide + Wind	34	4.6 **(90th)**	–	–	–
M-3	Tide + Wind	236	4.2 **(50th)**	–	–	–
M-4	Td + Wd + Waves	236	4.2 **(50th)**	214	0.51 **(50th)**	6.5
M-5	Td + Wd + Waves	236	4.2 **(50th)**	214	0.51 **(50th)**	9.8
M-6	Td + Wd + Waves	236	6.7 **(90th)**	214	1.22 **(90th)**	6.5
SE-1	Tide + Wind	169	2.9 **(50th)**	–	–	–
SE-2	Td + Wd + Waves	169	8.1 **(90th)**	169	0.96 **(90th)**	5.6
M-EW(*)	Td + Wd + Waves	34	2.1 **(50th)**	236	0.51 **(50th)**	6.5

Moreover, the presence of a counterclockwise rotating eddy in the southern part of the nearshore gives rise to a "rip current" (dot curve in panels a, b, and c) that flows adjacent to the most contaminated areas of the seabed (Figure's background). The eddy is obviously created by the domain's boundary that acts as a streamline.

Only during the infrequent "SE" attacks, the flow regime becomes fully cyclonic (Fig. 5, panel d) and therefore incompatible with the observed pollution pattern.

2.2. Delft3D-PART and related parameters

Delft3D-PART equates the movement of contaminants in water (dissolved or suspended) with that of a large number of particles subject to advection, dispersion, and settling.

Advection is calculated by elaborating the outputs of Delft 3D-FLOW in a Lagrangian framework, so the particle's position is independent of the grid resolution. The random walk approach models the horizontal and vertical dispersion (see e.g. Ibe, 2013), while a user-defined value for the fall velocity, w_s, controls the settling.

During the motion, the particles entering the bottom layer can remain on the seabed, thereby inducing contamination, or be reflected in the water column; this depends on whether the instantaneous shear stress, calculated through the well-known Chezy formula (see Appendix A.I), falls below a threshold value, $\tau_{b,sed.}$

The degree of seabed contamination can finally be calculated by counting the number of particles resting in the bottom layer at the end of each simulation.

The reader may find more details in Appendix A.I.

2.3. PART's governing parameters

Because Delft3D-PART is based on a relatively simple approach, it requires a smaller number of parameters than other water quality models; this makes the simulations somewhat less dependent on possible subjective decisions by the modeler.

The parameters to be assigned can be conveniently gathered into three groups:

1. particle-related parameters;
2. inflow-related parameters;
3. nearshore-related parameters.

In what follows, we briefly summarise the criteria that led to the selection of the values used, leaving a detailed discussion to Appendix A. II.

2.3.1. Particle-related parameters

This group of parameters includes (Table 2):

– nature of particles, i.e. what the particles are meant to represent;

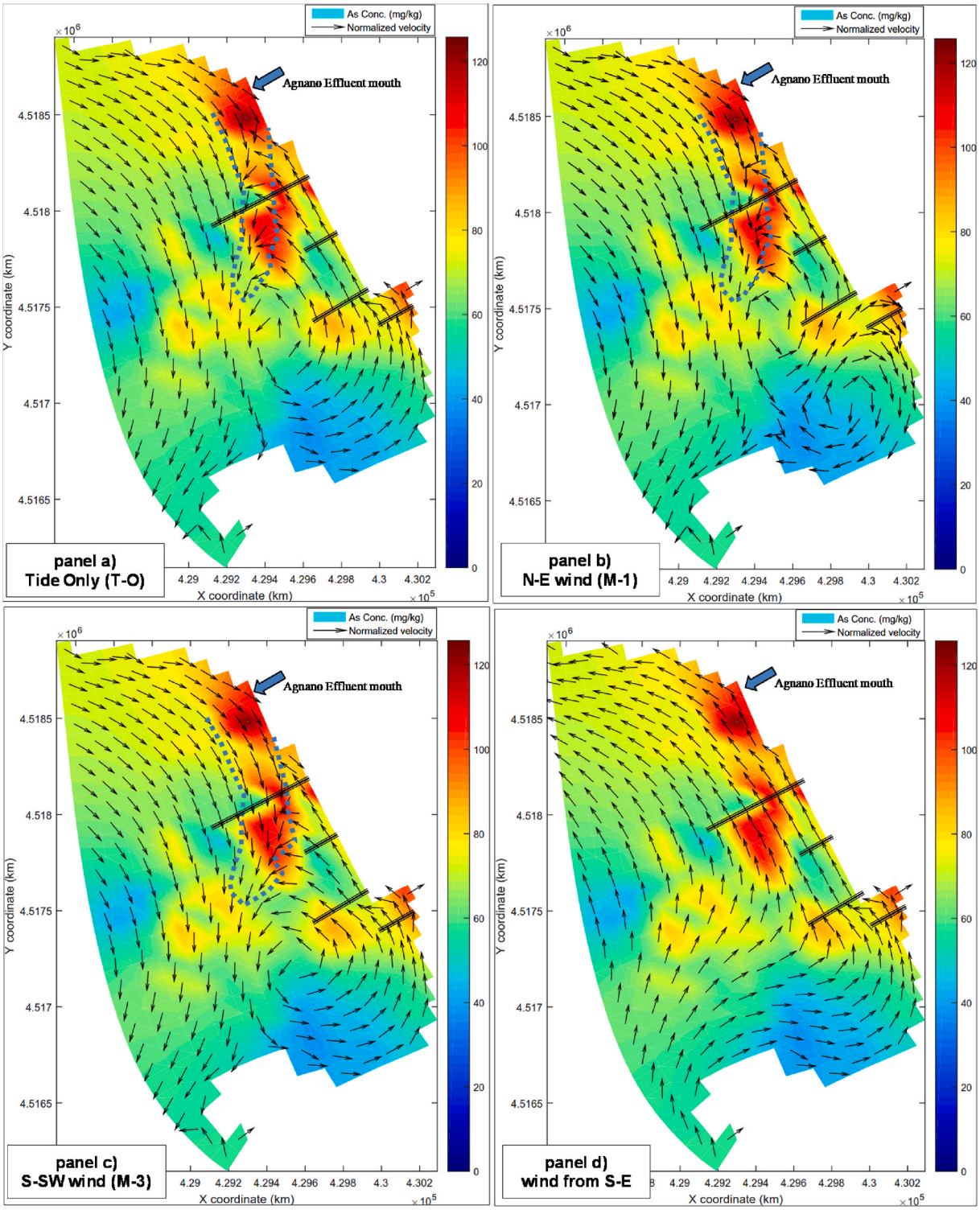

Fig. 5. Current regimes at the Bagnoli bay, according to Buccino et al. (2021). CSs refer to Table 1. The dotted line indicates rip current. Arsenic concentration is used as background.

– particle's settling velocity, w_s;
– limit bottom shear stress for deposition, $\tau_{b,sed.}$

Delft3D- PART does not simulate partitioning, so the nature of the particles must be specified a priori. In this study, two hypotheses were formulated, namely:

a) the particles represent arsenate anions in solution, potentially adsorbing to the bottom;
b) the particles represent fine sediments in suspension, to which As had previously adsorbed.

The above hypotheses rely on the fact that most of the arsenic in the CFc groundwater is in the +5 oxidation state (Aiuppa et al., 2006), which favors adsorption to various sediment minerals. Moreover, the

Table 2
Particle-related parameters.

Nature of particles	w_s [m/s]	$\tau_{b,sed}$ [N/m^2]
Arsenate anions	10^{-15}	$\left[\frac{\rho g}{C_h^2}\cdot(0.001)^2\right]^{(*)}$
5 μm silt grain	$2.25\cdot10^{-5}$	0.028

(*) values of C_h are calculated according to Table 4.

assumption of arsenic adsorbed on wash-load particles is consistent with the positive correlation found between this metalloid and aluminum, which is meant to represent aluminosilicates in the finest fraction of the sediments (Armiento et al., 2020; Somma et al., 2021).

In case a), the settling velocity is practically zero, and adsorption to the seabed occurs when the flow speed is smaller than 1 mm/s (Li et al., 2018).

In case b), $\tau_{b,sed}$ equals the limiting shear stress for the incipient motion of the sediments calculated by Miller's formula (1977). Since the formula is valid in the size range 4–250 μm (van Rijn, 2007), a particle diameter of 5 μm has been subjectively selected; w_s is calculated by **Stokes'** law.

2.3.2. Inflow related parameters

The inflow-related parameters (Table 3) concern the discharge of the Agnano Effluent, Q_{in}, the arsenic concentration at the mouth, c_{mth}, and the initial dispersion radius R_d, i.e. the dispersion of the pollutant immediately after release into the sea.

Different values of Q_{in} and c_{mth} have been used for winter and summer. In winter, the flow rate is the average of the measurements taken over between 2021/02/18 and 2021/03/20 (Fig. 4), while c_{mth} was derived from ad hoc analyses conducted at the laboratory of Sanitary Engineering of the University of Naples Federico II (mean concentration). Interestingly, water quality analyses didn't detect the presence of nitrates, indicating a limited contribution from wastewater.

In summer, Q_{in} corresponds to the discharge measured on 2021/06/07, after 23 consecutive days with no rain (red triangle in Fig. 4). Since no direct information was available on c_{mth}, it was assumed that the arsenic influx (i.e. the product Q_{in} x c_{mth}) were constant.

For R_d, a value of 5 m was used, which is typical of an initial outflow field formed over a marine outlet (Riddle and Lewis, 2000).

The numerical simulations last 30 days, during which the inflow is continuous and occurs at the uppermost layer of the computational domain (water surface). Since the minimum computational cell has a 3139 m^2 horizontal surface, and the bottom layer thickness is of the order of 1 m, 2×10^5 particles have been used, which gives a concentration resolution of nearly 0.054 μg/l. This value is about 5% of the arsenic concentration at the inlet; a further increase in the particles' number (up to 2×10^6) did not produce any significant variation in the numerical results.

2.3.3. Nearshore-related parameters

This group (Table 4) encompasses:

- the climate scenario (CS);
- the Chezy coefficient, C_h, for shear stress calculation;
- the horizontal and vertical dispersion coefficients, D_{xy} and D_z;

Among the CSs of Table 1, we don't consider "SE" attacks, since the cyclonic circulation they produce (Fig. 5) is inconsistent with the observed arsenic pollution pattern.

Table 3
Inflow related parameters.

Q_{in} [l/s]		c_{mth} [μg/l]		R_d [m]
Winter	Summer	Winter	Summer	
237	130	100	182	5

Table 4
Nearshore-related parameters. (*) RMS value between 0.5 and 10 m.

Scenario	$C_h^{(*)}$ [m$^{1/2}$/s]	D_{xy} [m^2/s]	D_z [m^2/s]	
T-O	60.5	1.00	Winter	*Summer*
M-1	64.9			
M-2	64.9			
M-3	64.9			
M-4	47.1		$10^{-4} \div 10^{-3}$	$10^{-6} \div 10^{-5}$
M-5	47.1			
M-6	58.3			
M-EW	47.1			

The Chezy coefficients were calculated by introducing some simplifications to the method of van Rijn (2007). Consevatively, the entire shear stress is considered; with increasing hydrodynamic forcings (e.g. passing from T-O to M-1), the friction reduces because of the transition from "*stable-ripples*" to "*sheet-flow*". Moreover, in the presence of waves C_h diminishes significantly, as the interaction between waves and currents results in the formation of a double logarithmic boundary layer. This because any source of turbulence is assumed to hinder sedimentation.

D_{xy} and D_z are order of magnitude estimates obtained from the literature (Okubo, 1971; Kullenberg, 1971). Readers may refer to Appendix A.II for more details.

The vertical dispersion coefficient differs between winter and summer due to the stratification of the water column observed in the Bagnoli bay, as well as the entire south Tyrrhenian sea, during the warm season (Castagno et al., 2020).

In the simulations, D_{xy} is kept constant, whereas D_z is varied within the ranges of Table 4.

3. Results

3.1. Approach

The numerical experiments lasted 30 days, which is much less than the 160 years during which the Agnano Effluent is discharging water into the sea. Therefore, the results presented below are necessarily qualitative and focus on the shape of the contamination patterns rather than the pollution magnitude. The seabed arsenic concentrations resulting from Delft3D-PART are compared to the measurements in a standardized form, i.e. subtracting the mean value across the computational domain, and dividing by the standard deviation. The measurements used for comparison (Fig. 3) were carried out in the frame of the ABBaCo research project (Morronid'Errico et al., 2020), using 98 cores from one to 4 m in length. The cores were distributed across the bay according to Fig. 6.

3.2. Contamination patterns under summer conditions

3.2.1. Arsenate anions (case a)

Since particles are released at the water surface and have practically no settling velocity, their motion is particularly affected by the wind drag, as well as the "rip current" shown in Fig. 5. Moreover, the contamination patterns depend strongly on the vertical dispersion coefficient D_z, as it rules the probability of a particle reaching the bottom layer; the larger D_z is, the greater the probability of pollution. Finally, attachment to the seabed is obviously favored by low values of bottom shear stress.

Under the CSs M-1 and M-2 (Fig. 7), the wind drag acts in the same direction as the rip current, pulling the particles far from the inlet. Only when the wind speed is low (M-1), and D_z is large enough (panels b and c), some contamination at the AE mouth is observed.

On the other hand, with mild winds blowing from S-SW (M-3, Fig. 8),

Fig. 6. Scheme of the cores employed within the ABBaCo project.

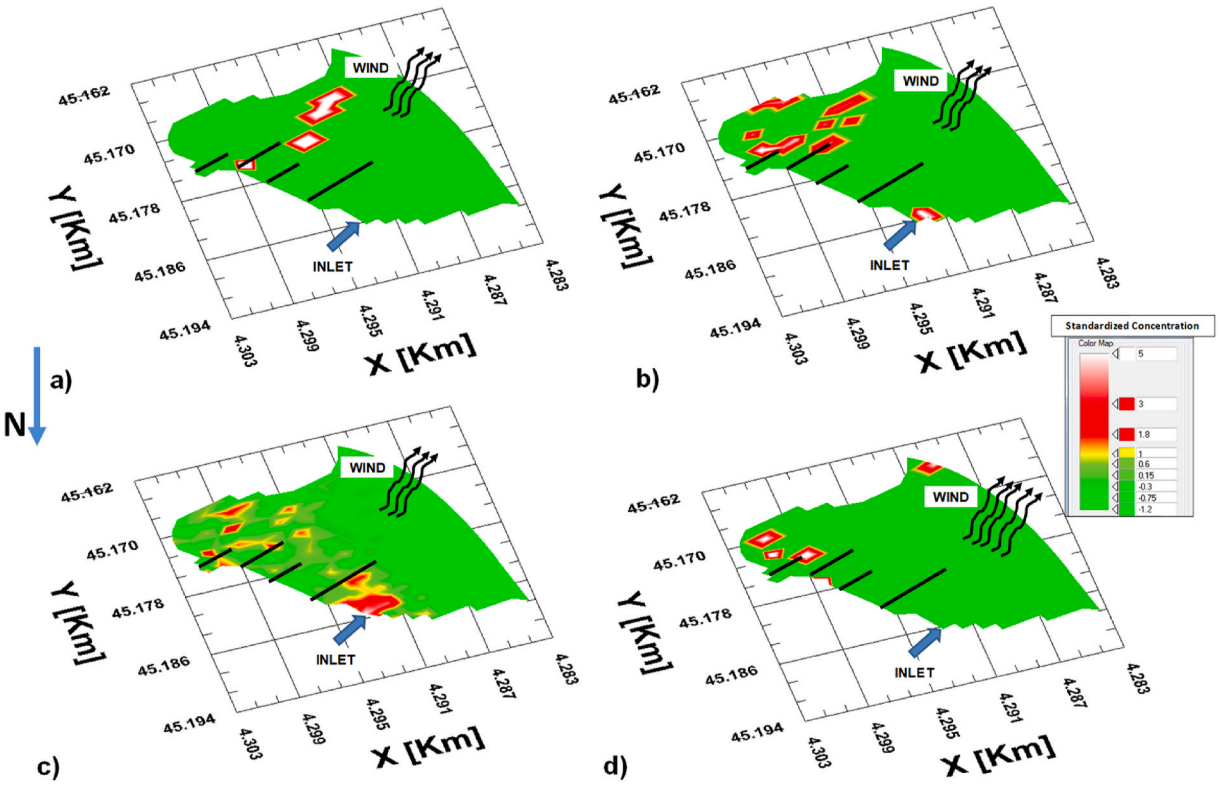

Fig. 7. Numerical contamination patterns at the seabed (standardized), under N-E winds. Panel a):M-1, $D_z = 5 \times 10^{-6}$ m^2/s; Panel b):M-1, $D_z = 1 \times 10^{-5}$ m^2/s; Panel c):M-1, $D_z = 2 \times 10^{-5}$ m^2/s; Panel d):M-2, $D_z = 2 \times 10^{-5}$ m^2/s.

the drag reversal keeps the particles in the nearshore, leading to pollution contours consistent with measurements; as shown in Fig. 8, this result is qualitatively independent of the value of the vertical dispersion index.

Adding waves to the westerly wind increases the rip's strength, as one observes comparing panels a) and b) of Fig. 9; at the same time the bottom shear stress grows up due to the wave-current interaction, and the Chezy coefficient reduces considerably (Table 4). These two mechanisms overwhelm the "keeping effect" of the wind drag and lead pollution to occur far from the piers (panels c and d in Fig. 9).

It is however of interest that particles are pulled towards areas that suffer from arsenic concentrations relatively high. A similar feature was also observed in Fig. 7 for NE winds. This might indicate that AE could impact the contamination of sediments even beyond the piers region in

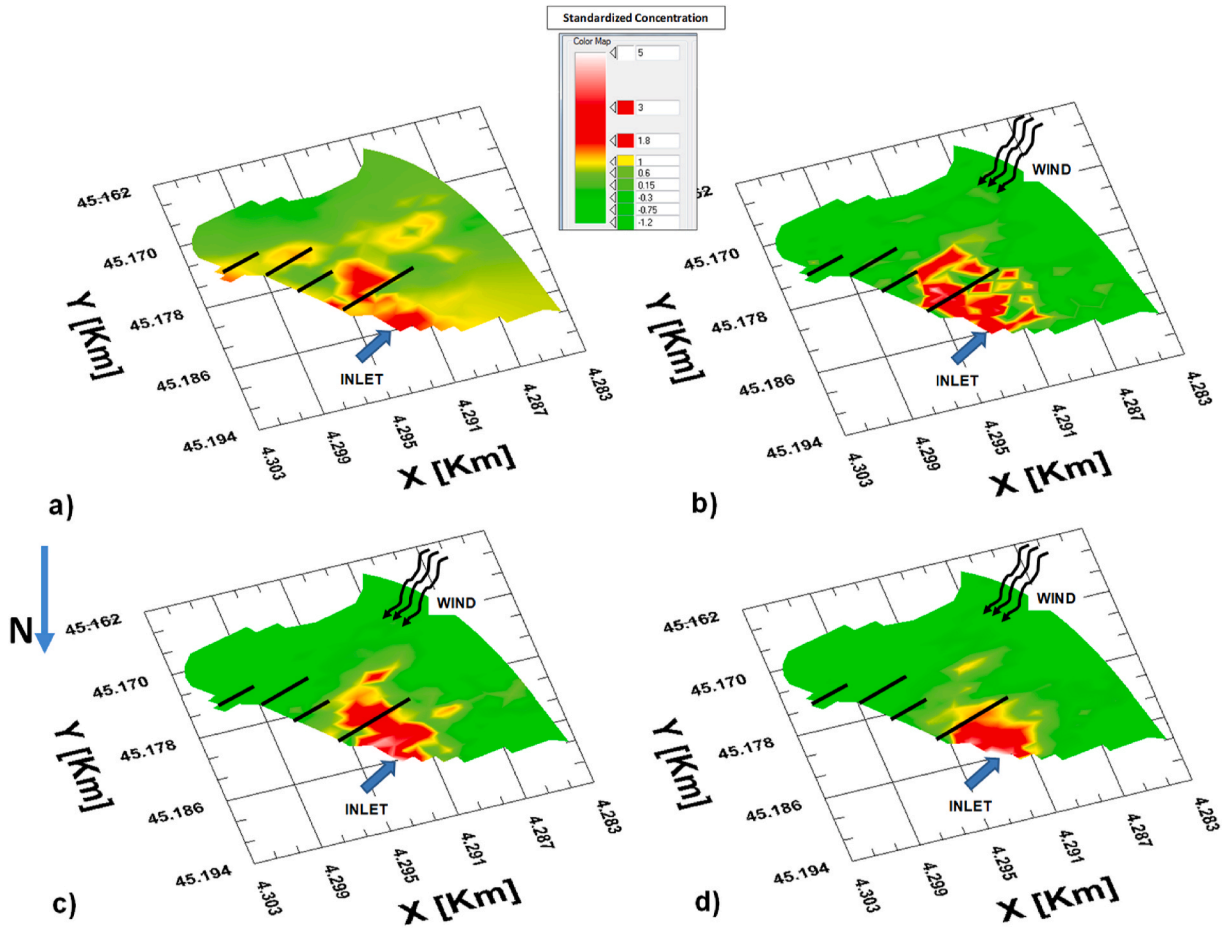

Fig. 8. Panel a): measured contamination patterns (standardized values between 0 and 50 cm). Panels b)-d): numerical simulations under M-3. Panel b): $D_z = 5 \times 10^{-6}$ m^2/s; panel c): $D_z = 1 \times 10^{-5}$ m^2/s; panel d):M-1, $D_z = 2 \times 10^{-5}$ m^2/s.

the central part of the bay.

3.2.2. *Particles simulating 5 μm silt grains*

When particles represent contaminated silt grains, the settling velocity (w_s) is no longer zero, and, accordingly, the wind stress has a lesser influence on their motion.

Moreover, the limiting stress for deposition, $\tau_{b,\,sed}$, increases dramatically, as shown in Fig. 10 for scenario M-1. The graph maps the logarithmic shear stress ratio:

$$L_\tau = log\left(\frac{\overline{\tau_b}}{\tau_{b,sed}}\right) \quad (1)$$

where $\overline{\tau_b}$ indicates the time-averaged bottom shear stress calculated through the Chezy equation. From "arsenate anions" (panel a) to "silt grains" (panel b), L_τ reduces up to three-four unities, that is the ratio between $\overline{\tau_b}$ and $\tau_{b,\,sed}$ reduces by 3–4 orders of magnitude.

The strong reduction in L_τ and the effect of w_s favor the deposition of the contaminated particles in the neighborhood of the AE mouth; for a vertical dispersion index as large as 2×10^{-5} m^2/s, all the CSs create pollution patterns that match with the measures (Fig. 11). Differently from what was observed for the arsenate anions (Figs. 7 and 9), the agreement is reasonable also under NE winds (panel c), and in the presence of waves (panel d). Although not shown here for sake of brevity, the role of wave period (M-4 vs. M-5) and wind direction (M-4 vs. M-EW) on the pollution patterns produced by waves was found to be secondary. This will be clearer in the following of the paper, from the inspection of Table 5 where all the scenarios affected by mild waves are seen to give the same correlation degree with measurements.

3.3. *The effect of winter storms*

Although D_z increases by an order of magnitude or two in winter, the shape of the numerical pollution patterns does not change macroscopically compared to the summer season; the exception is that NE winds now cause arsenate anion particles to rest near the inlet (Fig. 12), similar to what is observed for silt grains.

Scenario M-6 deserves a separate discussion, as it represents a low/medium intensity southwesterly storm that was not considered in Section 3.1.

Panel a) in Fig. 13 shows that where the particles simulate arsenate anions, no contamination occurs, however large D_z may be; this is because the intense bottom shear stresses prevent adsorption.

On the other hand, the silt grains form a polluted zone at the offshore tip of the piers (panels b and c) whose location and shape resemble the contamination contours 50–100 cm below the seafloor (panel d).

This may suggest that arsenic carried to the centre of the bay during winter storms is partly contributing to the pollution in the uppermost sediment layer, and partly subject to a burial process, the nature of which is however still unknown. A burial amounting to 30% of the total pollution load was previously hypothesized by Daliri et al. (2020), in a preliminary study of the bay conducted with the Delft-3D WAQ module.

Of course, the burial may be associated with wave-triggered sediment transport, which occurs either alongshore or cross-shore. In this respect, the nearshore area can be conveniently divided into a "littoral zone", where sediments are dominantly suspended, and a "shoal zone" in which bedload prevails (Hallermeier, 1981). While littoral zone sediments move either alongshore or cross-shore (in the offshore direction), the shoal zone is dominated by a landward-directed

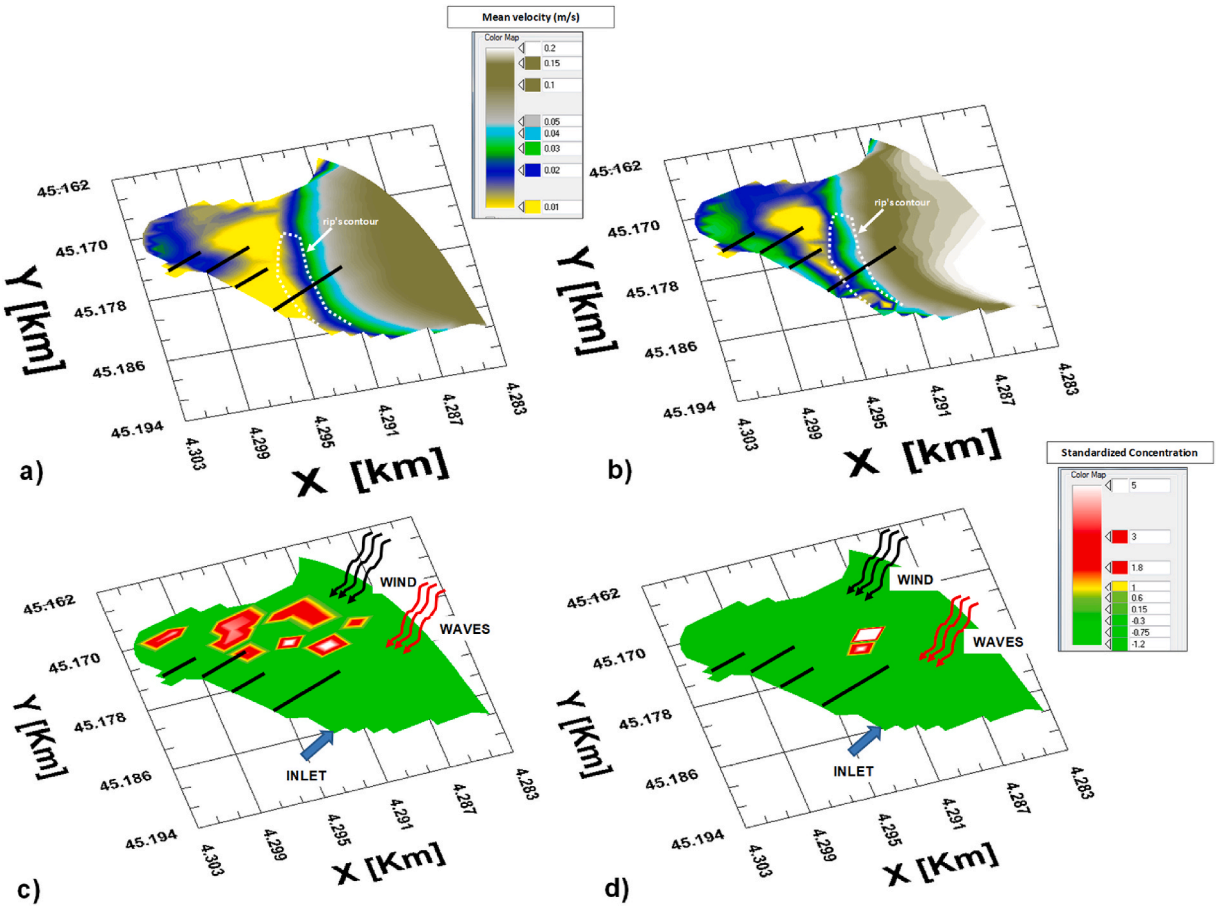

Fig. 9. Depth-integrated time-averaged flow velocity map for M-3 (panel a) and M-4 (panel b). Dotted curves represent the rip current of Fig. 4. Panels c)and d): numerical contamination patterns under M-4 and M-5. $D_z = 2 \times 10^{-5}$ m^2/s.

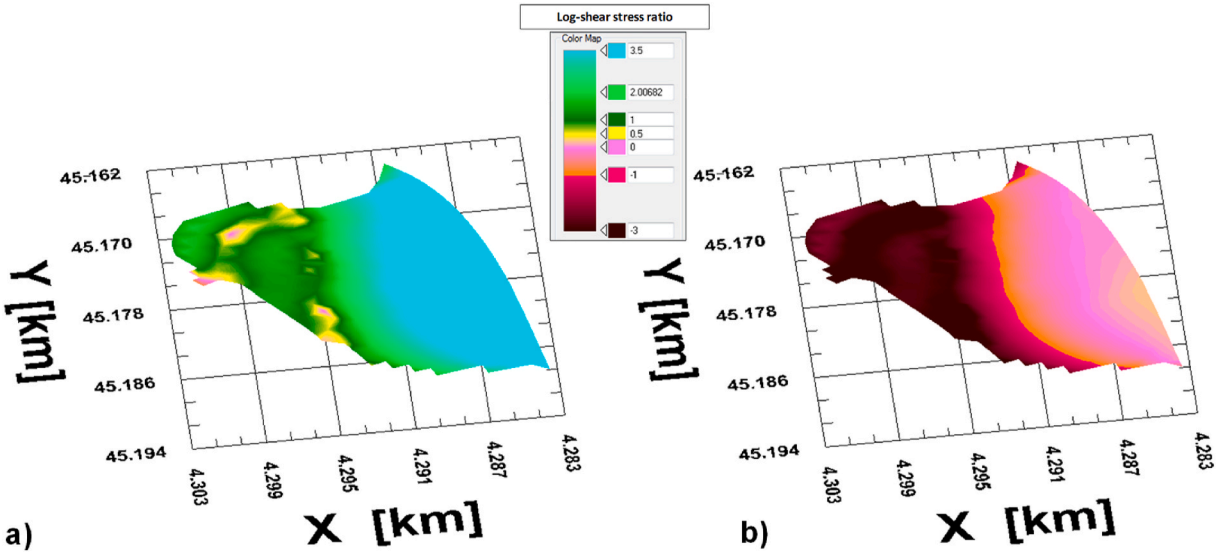

Fig. 10. Contours map of L_τ for M-1. Panel a):arsenate anions; panel b): 5 μm silt grains.

cross-movement. Within the ABBaCo project, the authors showed the littoral zone of the Bagnoli bay to hardly exceed 4.0 m water depth, which is too shallow to explain the burial process here hypothesized. On the other hand, the shoal zone may extend beyond 20 m, which might lead the offshore un-contaminated sand to cover polluted areas formed under winter storms.

4. Discussion

To have a more in-depth view of the results presented above, it is useful to look at them again from a quantitative perspective. To this end, we use simple linear regression analyses; the arsenic concentrations measured at the 92 cores in Fig. 6 (0–50 cm) represent the output

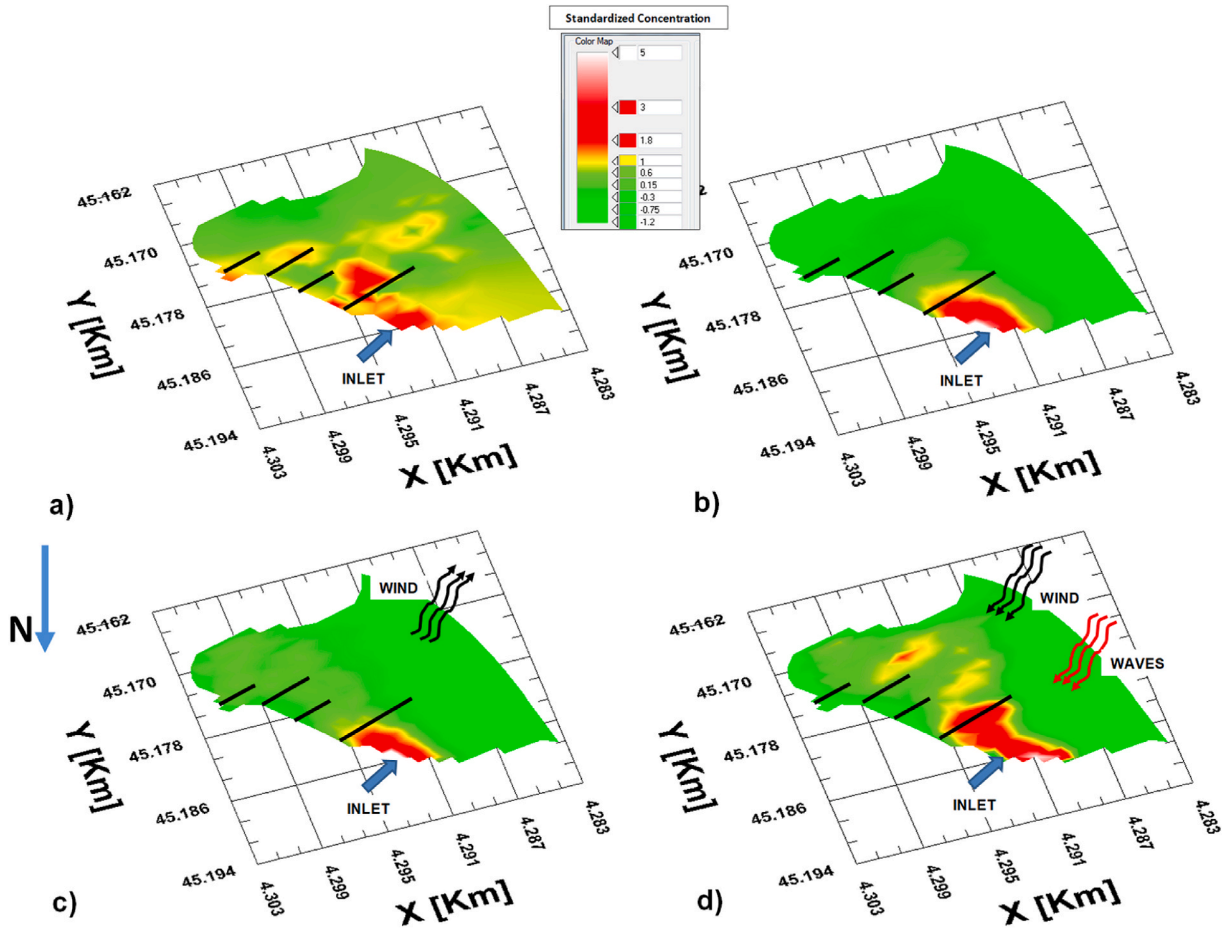

Fig. 11. Panel a): measured contamination patterns (standardized values between 0 and 50 cm). Panels b)-d): numerical simulations under T-O, M-1 and M-5. $D_z = 2 \times 10^{-5}$ m^2/s.

Table 5
Correlation coefficients under different climatic scenarios for Summer conditions.(*) average Pearson's correlation coefficients among the discharges North of the main pier.

CS	Arsenate Anions		Silt 5 μm	
	Summer $D_z = 2\ x\ 10^{-5}$ m$^2/s$	Winter $D_z = 1\ x\ 10^{-4}\ m^2/s$	Summer $D_z = 2\ x\ 10^{-5} m^2/s$	Winter $D_z = 1\ x\ 10^{-4}\ m^2/s$
T-O	0.49	0.49	0.53	0.49
M-1	n.s.		0.48	
M-2		0.49		0.48
M-3	0.53		0.51	
M-4	n.s.	n.s.	0.38	0.37
M-5	n.s.	n.s.	0.41	0.39
M-EW	n.s.	n.s.	0.39	0.37
M-6		n.s.		n.s.

variable (Y), while the numerical values at the same points, for each scenario, serve as the predictor (X).

The inflow of thermal water from AE is assumed to affect the pollution of the seabed if, for some CSs, there is a (positive) linear relationship between X and Y, which is significant at a 0.05 test level (Draper and Smith, 1981).

From a methodological point of view, it is worth mentioning that since Delft3D-PART simulates the dispersion process stochastically, the numerical experiments were repeated 30 times for each scenario, and the resulting concentrations at the bottom were then averaged point by point.

Results of the regression analyses are summarized in Table 5, which gives the values of the correlation coefficient, *R*, for winter and summer; the code "n.s." denotes "non-significant" regressions.

Summer conditions are simulated by the "50th percentile" climate scenarios of Table 1 (M-1, M-3, M-4, M-5, M-EW), while the winter season encompasses all wave-forced CSs (M-4, M-5, MEW, M-6), as well as M-2 (90th percentile NE wind). Noteworthily, T-O was considered either in winter or in summer.

From a hydrodynamic point of view, the most relevant result is that the tidal circulation (T-O) gives an almost constant value of R (≈ 0.50), regardless of the season and the nature of particles. The presence of wind and waves can possibly cancel this correlation (as in the case of waves for arsenate anions) but not increase it significantly. Hence, tidal currents can be considered the most important hydrodynamic driver for the contamination process, which also acts continuously over time. As shown in Fig. 14, there is a reasonable agreement between numerical simulations and measurements northwest of the main pier (left panel),

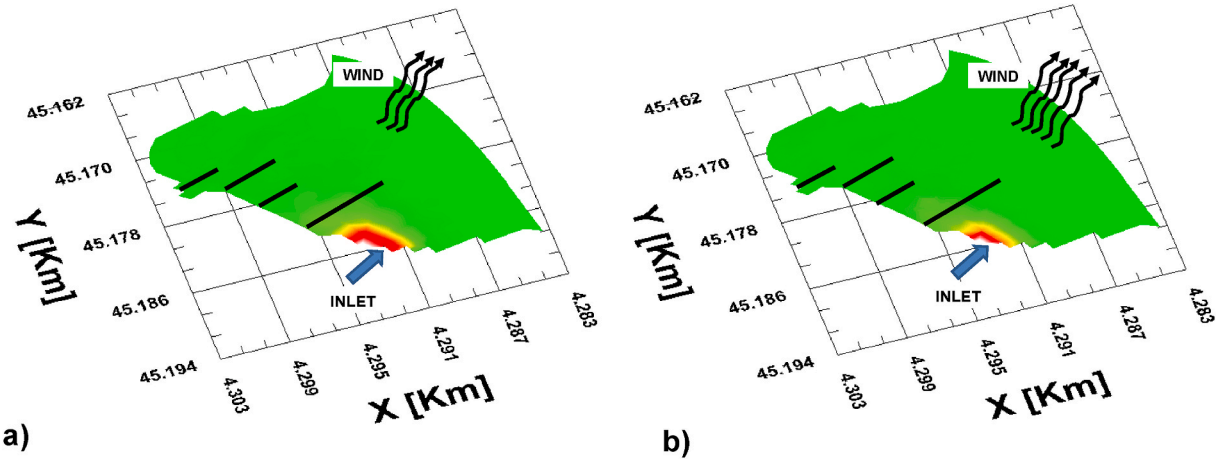

Fig. 12. Numerical contamination patterns at the seabed under N-E winds for arsenate anions. Panel a):M-1; panel b):M-2. $D_z = 1 \times 10^{-4}$ m^2/s.

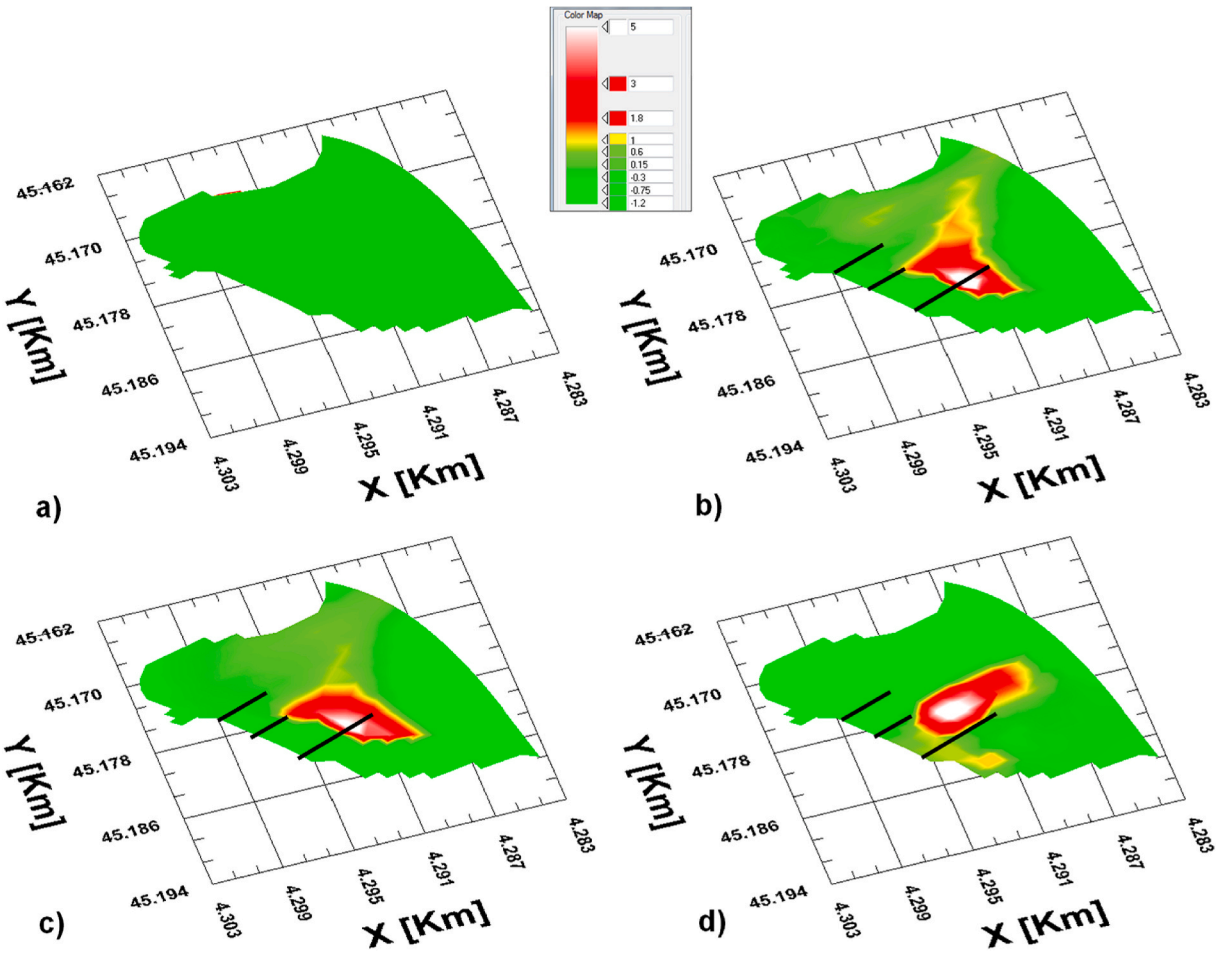

Fig. 13. Standardized bottom contamination patterns for M-6. Panel a): particles represent arsenate anions ($D_z = 3\ 10^{-3}$ m^2/s); Panels b) and c): particles represent 5 μm silt grains ($D_z = 2\ 10^{-4}$ and $3\ 10^{-3}$ m^2/s, respectively); Panel d: measured As concentration 50–100 cm beneath the seafloor.

while the correlation is poor either offshore or in the southeast direction (right panel).

The fact that the regressions for 5 μm silt grains are significant for all CSs (except M-6), confirms that seabed pollution patterns consistent with measurements are much more likely in the presence of abundant wash-load particles (silt grains but also clay minerals, oxydriles, etc). In this regard, it is of interest that Castagno et al. (2020) measured substantial turbidity levels at the water surface during the warm season (Fig. 15 a), and explained this just as the effect of some drain discharge. Fig. 15a) also shows that in the neighborhood of the AE mouth, high turbidity areas have approximatively the same shape as the rip current in Fig. 5.

As stated above, the presence of waves tends to reduce the degree of correlation; the latter is completely nullified in the case of arsenate anions, while R keeps a value around 0.4 for silt grains (M-4, M-5, M-EW); such a value is almost independent of wave period and wind

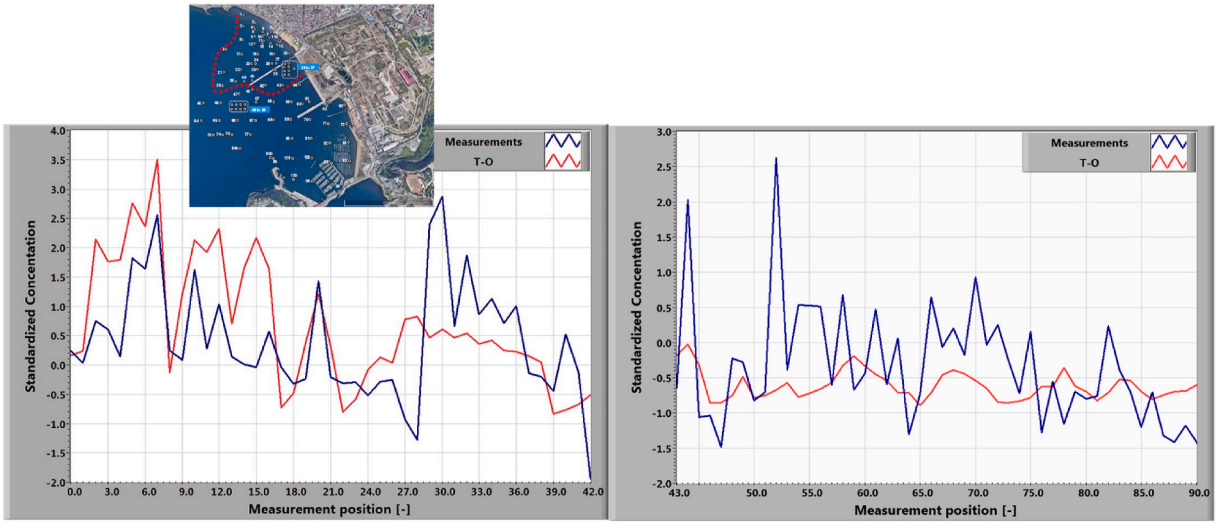

Fig. 14. Comparison between numerical and measured (standardized) concentrations for scenario T-O. Silt grains with $D_z = 2 \times 10^{-5}$ m^2/s. Left panel: cores 1–42 (red broken line in the upper box). Right panel: cores 43–90. (For interpretation of the references to colour in this figure legend, the reader is referred to the Web version of this article.)

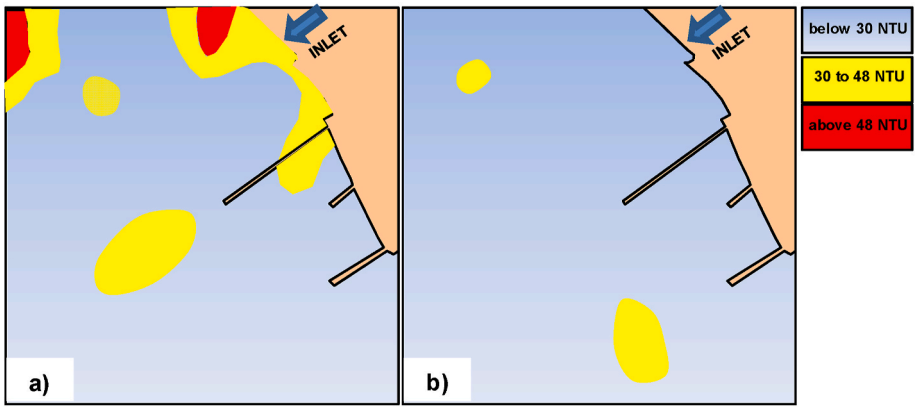

Fig. 15. Qualitative sketch of high turbidity areas at the water surface according to Castagno et al. (2020). Panel a): summer conditions (2018/06/21). Panel b): winter conditions (2018/12/07); superficial turbidity reduces due to strong vertical dispersion.

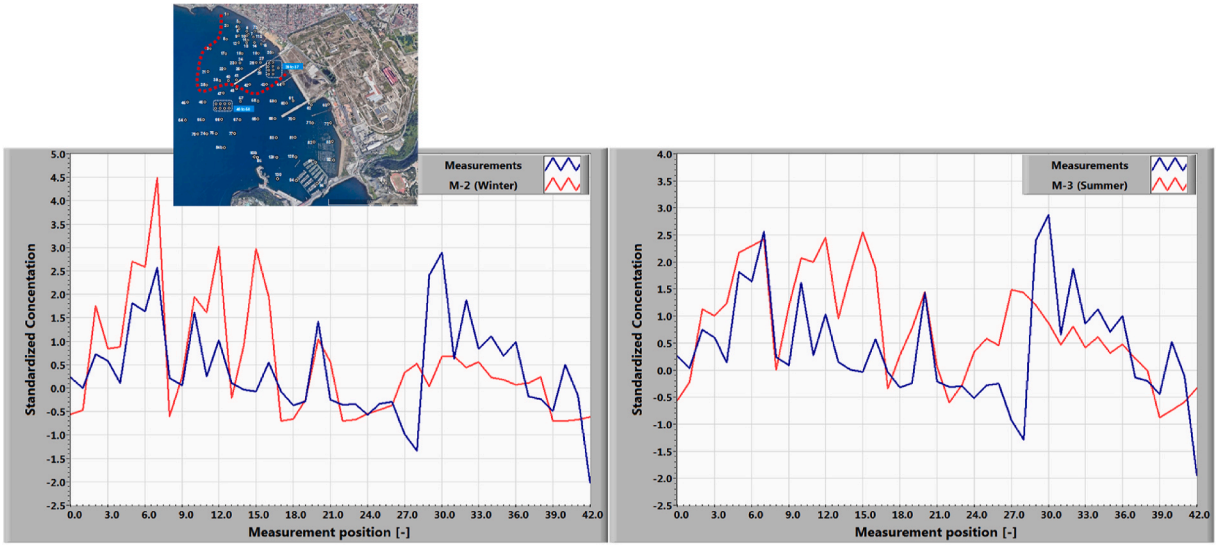

Fig. 16. Comparison between numerical and measured (standardized) concentrations for Arsenate anions. Left panel: M-2 in winter ($D_z = 1 \times 10^{-4}$ m^2/s). Right panel: M-2 in summer ($D_z = 1 \times 10^{-5}$ m^2/s).

direction.

It is also worth mentioning that in the case of arsenate anions, R retains a value of approximately 0.5 under two conditions rather frequent for the Bagnoli bay, namely mild S-SW winds in summer and NE winds in winter (Fig. 16).

Therefore, one reasonably argues that the Agnano Effluent plays a significant role in the pollution of marine sediments, but the approach here employed prevents achieving a global indicator of its impact.

Notwithstanding, recognizing tidal circulation as the primary driver of the process, we may tentatively take $R \approx 0.50$ as a representative value, meaning that influx of thermal water from AE explains about a quarter of the As concentration variability across the bay.

This hypothesis is consistent in magnitude with the results of the PCA analysis by Giglioli et al. (2020), who argued that discharges located at the westerly side of the Bagnoli bay can affect the seabed arsenic concentration by a factor of about 1/3 on average (average $R = 0.57$).

Before concluding this section, it is useful to remark that the results here presented are strictly dependent on the several hypotheses formulated in the numerical analysis. Among them, the main physical assumptions are certainly the absence of resuspension and the constant size of the wash load particles. The impact of those assumptions will form the basis of future research work.

Preliminary analyses have shown that a resuspension limit stress identical to $\tau_{b,sed}$ elongates the pollution patch between the piers (as expected), leading to contamination contours more similar to the measures. An example is shown in Fig. 17 for 5 μm silt grains under scenario M-4, where the resuspension is observed to push particles towards the polluted areas in the eastern part of the bay, similar to what was observed for arsenate anions under NE winds (Section 3.2.1).

On the other hand, reducing the wash load particle size has a limited effect on the pollution pattern under tide and wind stress only, while the presence of waves tends to increase the correlation degree around the northernmost pier (cores 20 and 40 of Fig. 6). An example is shown in Fig. 18 for the case of clay mineral particles with a 0.3 μm diameter.

Neither resuspension nor particle size, however, seem to affect significantly the quantitative conclusions of this study.

5. Conclusions

A particle tracking numerical model (Delft3D-PART) included in the software package Delft-3D, has been used to investigate whether, and to what extent, the arsenic released from an artificial channel in the westernmost part of Bagnoli bay could affect the contamination of marine sediments. The artificial channel is referred to as the "Agnano Effluent" (AE, Fig. 3).

Although previous studies provided indirect evidence on the role of AE, no attempt was ever made to numerically reproduce the contours of contamination on the seabed to compare with measurements.

The approach adopted in this research introduces several crude simplifications, namely:

- climate forcings are quasi-stationary combinations of wind waves and tides (*climate scenarios*);
- dispersion and settling processes are governed by simple coefficients (dispersion indexes, settling velocity);
- duration of the numerical experiments is much less than the real contamination process time-scale.

Moreover, the partitioning of the arsenic released into the water is accounted for by two a priori assumptions on the nature of the particles; they represent either arsenate anions in solution or wash-load particles to which arsenic had previously adsorbed.

In spite of those limitations, however, a number of interesting conclusions could be drawn, which can be summarized as follows:

a) The transfer of contaminants from AE to the marine sediments is primarily ruled by the tidal circulation, which acts as a background forcing continuously over time. Wind and waves can possibly cancel out the effects of tidal flows but have never been observed to enhance them significantly.
b) Generally, the presence of waves and/or NE winds tend to oppose the contamination in the area of piers, whereas mild winds from S-SW favor it slightly. However the particles are pulled to areas where the contamination is relatively high. This would indicate that AE could impact the pollution of marine sediments even beyond the central part of the bay.
c) the arsenic released is more likely to contaminate marine sediments in the presence of abundant wash-load particles, such as silt grains, clay minerals, oxydriles, etc. These conditions seem to occur primarily during the warm season, when Castagno et al. (2020) measured large turbidity values in the neighborhood of the AE inlet;

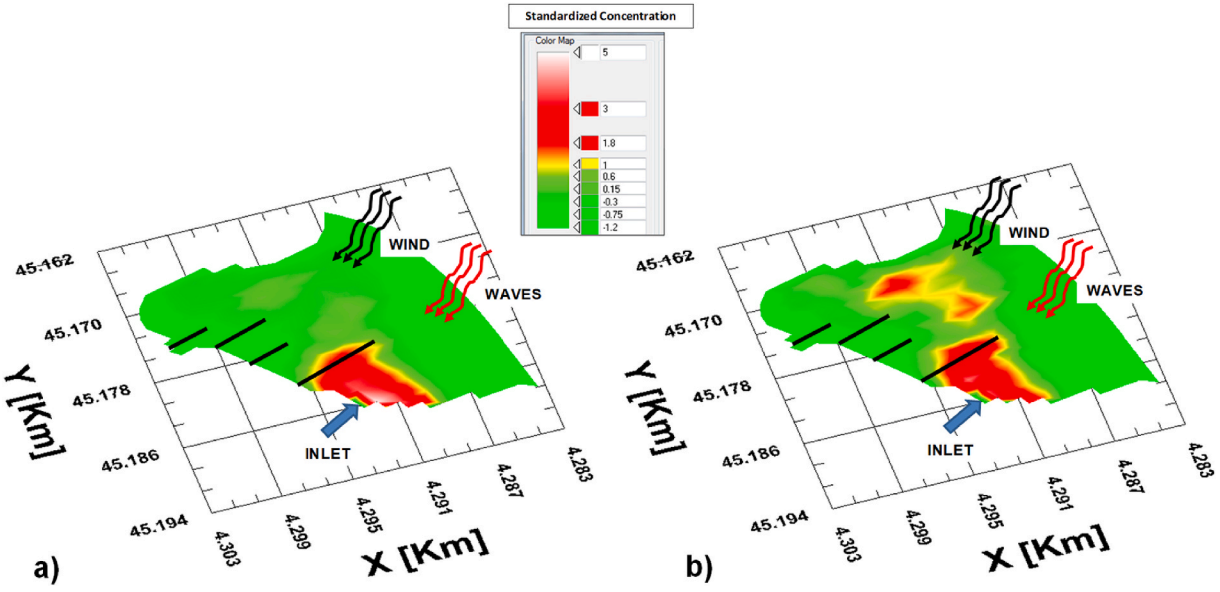

Fig. 17. Numerical contamination patterns for 5 μm silt grains under M-4 (summer conditions). Panel a):no resuspension; panel b): resuspension with limit stress equal to $\tau_{b,sed}$. $D_z = 2 \times 10^{-5}$ m^2/s.

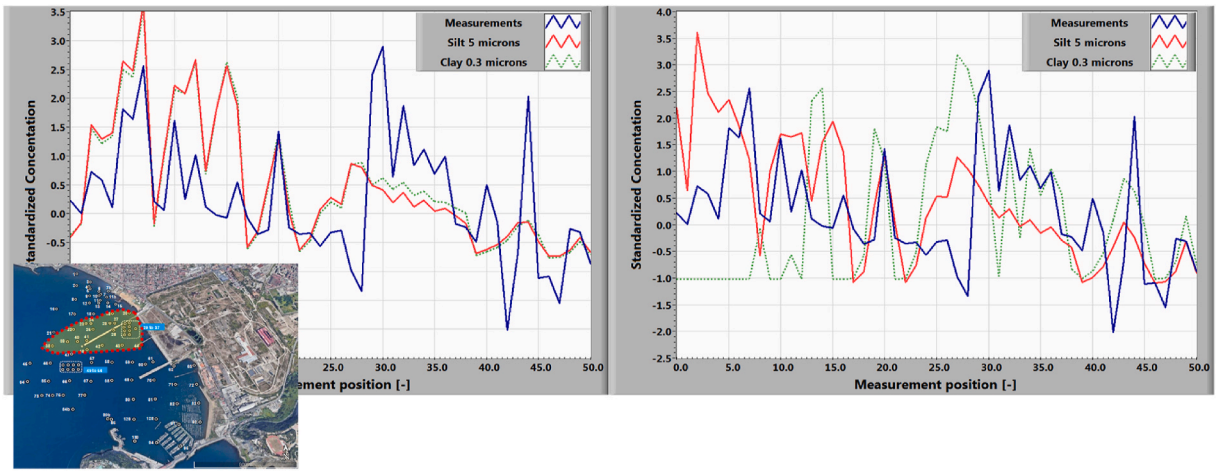

Fig. 18. Comparison between numerical and measured (standardized) concentrations for silt and clay mineral particles. Summer conditions with $D_z = 2 \times 10^{-5}$ m^2/s. Left panel: M-3; Right panel: M-5. Lower panel highlights the area between cores 20 and 40.

d) Assuming the tidal circulation to represent the leading hydrodynamic driver that enables the seabed pollution, we conclude, from simple regression analysis, that the release of thermal water from the Agnano Effluent impacts the overall arsenic contamination process by ¼, which is consistent with early literature based on multivariate statistics (Giglioli et al., 2020).

After reviewing the outcomes of all the most recent research studies (including this research), it was planned to divert the Agnano Effluent into a new drain that collects thermal water and wastewaters from the Agnano area and, conveys them to a sewage lifting plant at the border between the cities of Napoli and Pozzuoli.

Authors contribution

- Mariano Buccino: Conceptualization, Methodology, Writing-Original Draft.
- Mohammad Daliri: Software, Modeling Investigation.
- Norma Buttarazzi. Software, Investigation, Data curation.
- Giuseppe Del Giudice: Methodology, Investigation; Writing-Review.
- Mario Calabrese: Writing-Review, Data Curation.
- Renato Somma: Conceptualization, Formal Analysis, Data curation; Formal Analysis.

Declaration of competing interest

The authors declare that they have no known competing financial interests or personal relationships that could have appeared to influence the work reported in this paper.

Acknowledgments

This research results from a collaboration between the University of Naples Federico II and the National Institute of Geophysics and Vulcanology (INGV). The partnership is born in the frame of the multidisciplinary project ABBaCo, funded by the Italian Ministry of Education and Research, which aimed to provide innovative and environmentally friendly solutions for restoring the Bagnoli area. The authors wish to acknowledge Prof. Luigi Musco (ABBAcO's coordinator), Drs. G. De Natale and C. Troise (INGV), and M.S. engineers M.C. Ciccaglione and C. Di Costanzo (University of Naples Federico II) for helpful assistance.

Dr. Ludovico Pontoni and Prof. Giovanni Esposito (University of Napoli Federico II) are also gratefully acknowledged.

Appendix A.I. Details on Delft3d-part

For each time step, Delft-3D PART first calculates advection according to the equation:

$$x_j(t+\Delta t) = x_j(t) + \int_0^{\Delta t} \left(\frac{dx_j}{dt}\right) dt \tag{A.I.1}$$

where $x_j = x_j(t)$ is the j-th component of trajectory, and dx_j/dt indicates the respective Lagrangian velocity.

In this phase, the velocity field computed by the Delt 3D-FLOW module is integrated after a linear interpolation between the values at the borders of computational cells.

The horizontal and vertical dispersion components, ΔS_{xy} and ΔS_z, are then added to the trajectory. They are random quantities calculated as:

$$\Delta S_{xy} = [ran(-1, +1)]\sqrt{6D_{xy}\Delta t} \tag{A.I.2}$$

$$\Delta S_z = [ran(-1, +1)]\sqrt{6D_z\Delta t} \tag{A.I.3}$$

in which D_{xy} and D_z are the horizontal and vertical dispersion coefficients, Δt is the time step, and $ran(-1, +1)$ represents a random variable uniformly distributed in the interval (−1,+1).

The bottom shear stress, τ_b, is related to the depth-averaged flow velocity, U, via the 2D Chezy equation:

$$\tau_b = \rho g \frac{U^2}{C_h^2} \tag{A.I.4}$$

in which ρ is the water density, g is gravity, and C_h is the Chezy coefficient.

Appendix A.II. Selection of "Delft3d-part" parameters

A.II.I. Limiting shear stress for deposition, $\tau_{b,sed}$

When the particles represent arsenate anions dissolved into the water, adsorption to the bottom sediments is assumed to occur when the depth-averaged flow velocity, U, falls below a limiting threshold, say U_{lim}.

In the lack of clear indications from literature, a crude, conservative value of the order of magnitude of U_{lim} was derived from Li et al. (2018). The authors investigated the arsenate adsorption in a water flow passing through a cylinder filled with a porous composite of iron oxides and carbon. Adsorption was observed at flow rates between 3.43 and 15.41 cm^3/min, corresponding to U_{lim} of the order of 1 mm/s (between 0.5 and 2 mm/s).

In the case where particles represent 5 μm silt grains, $\tau_{b,\ sed}$ corresponds to the limiting shear stress for incipient motion suggested by Miller et al. (1977):

$$\frac{\tau_{b,\ sed}}{(\rho_s - \rho)\cdot g \cdot D_{sg}} = \begin{cases} 0.115 \cdot D_*^{-0.5} & D_* < 4 \\ 0.14 \cdot D_*^{-0.64} & 4 \le D_* < 10 \end{cases} \tag{A.II.1}$$

where ρ_s indicates the density of the grains (2700 kg/m^3), ρ is the water density, and the dimensionless grain size D_* equals:

$$D_* = D_{sg}\left[\left(\frac{\rho_s - \rho}{\rho}\right)\cdot\frac{g}{\nu^2}\right]^{1/3} \tag{A.II.2}$$

in which D_{sg} is the diameter of the silt grains and ν is the water's kinematic viscosity.

The Eq (A.II.2), which has been used by van Rijn (2007) in the range 4–250 μm, neglects the effects of cohesive forces.

It is worth noticing that in the Delft3D-PART, particles attached to the bottom may be re-suspended whenever the shear stress exceeds an upper limit value that leads to the bottom erosion. However, this process has not been considered in this study to ease the interpretation of results.

A.II.II. The Chezy coefficient, C_h

According to van Rijn (2007), the following equation has been used:

$$C_h = 18 \cdot log\left(\frac{d}{k_s}\right) \tag{A.II.3}$$

where d is the water depth, and k_s is the equivalent effective sand roughness height originally introduced by Nikuradse (1932). The roughness height has been equated to a multiple of the median bottom grain size, D_{50}:

$$k_s = r \cdot p \cdot D_{50} \tag{A.II.4}$$

with "*r" and "p"* depending on the flow resistance characteristics and the simultaneous presence of waves and currents. Conservatively, the entire shear stress is considered.

Under the "lower current regime", when the bottom ripples' form drag controls the flow resistance, $r = 150$; on the other hand, $r = 20$ in case of sheet flow (upper current regime), when the physical roughness is governed by the grains moving in a sheet layer near the bottom.

The coefficient "*p*" equals 1 in the absence of waves, while it reaches 10 for waves superimposed to currents due to the presence of a double "logarithmic layer" in the velocity profile (Fredsøe et al., 1999).

In the present study, $r = 150$ has been employed for the Scenario T-O, while $r = 20$ has been applied to M-6. An intermediate value of 85 has been chosen for the remaining cases, where ripples are likely stable in deeper waters and disappear in the nearshore.

It is worth highlighting that since the Delft3D-PART module requires only a single value of the Chezy coefficient, the Root Mean Square between -1m and −10 m (below MSL) has been used in the simulations; as per D_{50} a value of 0.15 mm has been taken as representative of the average sediment sizes at the Northern, Central, and Southern parts of the bay (see Table 3 in Buccino et al., 2021 and Molisso et al., 2020).

A.II.III. The horizontal dispersion coefficient, D_{xy}

The horizontal dispersion coefficient, $D_{xy,}$ has been estimated based on the predictive equation suggested by Okubo (1971):

$$D_{xy} = 0.0103 \cdot \lambda^{1.15} \quad \left[\frac{cm^2}{s}\right] \tag{A.II.5}$$

where λ (in cm) is the "scale of dispersion", i.e., the diameter of a circle containing 95% of the patch.

In the case of the Bagnoli bay, the scale of dispersion is realistically included between the length of the rip current in Fig. 7 (850 m), which encloses the high contamination contours, and the length of the entire computational domain (3.2 Km). These assumptions would lead D_{xy} to lie in the range

0.47–2 m^2/s, suggesting an intermediate value of 1 m^2/s.

It is noteworthy that a dispersivity of 1 m^2/s is order of magnitude consistent with the existing literature. As an example, Elliott et al. (1997) estimated a median value of 0.47 m^2/s in the coastal waters around Ireland, with a maximum of 1.69 m^2/s. On the other hand, Johnson and Pattiarachi (2004) provided the range 1.29–3.88 m^2/s for the total dispersion in a rip current's head.

A.II.IV. The vertical dispersion coefficient, D_z

Literature data on vertical dispersion spreads across several orders of magnitude.

In analyzing results of dye experiments along the UK coasts, Riddle and Lewis (2000) reported values ranging from 2 10^{-4} to 1.1 10^{-2} m^2/s; an even wider interval (5 10^{-6} and 1.1 10^{-2} m^2/s) was inferred by Kullenberg (1971).

Kullenberg (1971) also proposed the following formula, relating D_z to the main oceanographic variables:

$$D_z = 8.9 \cdot 10^{-8} \left(\frac{W}{N}\right)^2 \left|\frac{\partial U}{\partial z}\right| \tag{A.II.6}$$

where W is the wind speed (in cm/s), $\left|\frac{\partial U}{\partial z}\right|$ is the current's vertical gradient (current shear), and N represents the Brunt-Väisälä frequency:

$$N = \sqrt{-\frac{g}{\rho_0}\frac{\partial \rho}{dz}} \tag{A.II.7}$$

which is function of the water density gradient ($\partial\rho/\partial z$), relative to a reference value ρ_0.

The measurements carried out at the Bagnoli bay by Castagno et al. (2020) indicate the water column's characteristics undergo appreciable changes between winter and summer, which likely induces a significant seasonal variation on D_z.

In particular, the application of the Eckart (1952) formula to the measurements carried out on 2018/June/21 (Fig. 4 of Castagno et al.) leads to N = 0.33 Hz; therefore, since the average wind speed was 5.35 m/s (Buccino et al., 2021), and the current shear between 0 and -10 m was around 0.003 s^{-1} (Fig. 7), the Kullenberg formula gives $D_z = 7\ 10^{-6}$ m^2/s.

Conversely, winter measurements, taken on 2018/Nov/13 and 2018/Dec/7, show the water column to be almost un-stratified ($N \approx 0$) and featured with a rather barotropic flow $\left(\frac{\partial U}{\partial z} \cong 0\right)$. Hence, the vertical diffusivity during the cold season is realistically limited by the water depth, which can be used in Eq.(A.II.5) as "scale of dispersion". Accordingly, since the process under study occurs at less than 10 m, one may reason the vertical dispersion in winter does not exceed 3 10^{-3} m^2/s.

The values just inferred are not far from those detected at the Osaka bay (Japan) by Nishimura and Nakamura (1987) and Nakamura et al. (1991), who found typical D_z ranging from 2 to 5 10^{-5} m^2/s during the Summer and 1–2 10^{-4} m^2/s in Winter. On the other hand, Kullenberg (1971) measurements give average values of 2.2 10^{-5} m^2/s and 1.3 10^{-3} m^2/s, respectively, for the warm and the cold season.

References

Aiuppa, A., Avino, R., Brusca, L., Caliro, S., Chiodini, G., D'Alessandro, W., Favara, R., Federico, C., Ginevra, W., Inguaggiato, S., et al., 2006. Mineral control of arsenic content in thermal waters from volcano-hosted hydrothermal systems: insights from island of Ischia and Phlegrean Fields (Campanian Volcanic Province, Italy). Chem. Geol. 229, 313–330, 2006.

Albanese, S., De Vivo, B., Lima, A., Cicchella, D., Civitillo, D., Cosenza, A., 2010. Geochemical baselines and risk assessment of the Bagnoli brownfield site coastal sea sediments (Naples, Italy). J. Geochem. Explor. 105, 19–33, 2010.

Archetti, R., Lamberti, A., 2003. Assessment of risk due to debris flow events. Nat. Hazards Rev. 4 (3), 115–125. https://doi.org/10.1061/ASCE.1527-69882003_4:3115. ISSN: 1527-6988.

Armiento, G., Caprioli, R., Cerbone, A., Chiavarini, S., Crovato, C., De Cassan, M., De Rosa, L., Montereali, M.R., Nardi, E., Nardi, L., et al., 2020. Current status of coastal sediments contamination in the former industrial area of Bagnoli-Coroglio (Naples, Italy). Chem. Ecol. 36 (6), 579–597, 2020.

Buccino, M., Daliri, M., Dentale, F., Di Leo, A., Calabrese, M., 2019a. CFD experiments on a low crested sloping top caisson breakwater. Part 1. nature of loadings and global stability. Ocean Eng. 182, 259–282.

Buccino, M., Daliri, M., Dentale, F., Calabrese, M., 2019b. CFD experiments on a low crested sloping top caisson breakwater. Part 2. Analysis of plume impact. Ocean Eng. 173, 345–357.

Buccino, M., Daliri, M., Calabrese, M., Somma, R., 2021. A numerical study of arsenic contamination at the Bagnoli Bay seabed by a semi-anthropogenic source. analysis of current regime. Sci. Tot. Environ. 782.

Castagno, P., de Ruggiero, P., Pierini, S., Zambianchi, E., De Alteris, A., De Stefano, M., Budillon, G., 2020. Hydrographic and dynamical characterisation of the Bagnoli-Coroglio Bay (Gulf of Naples, Tyrrhenian sea). Chem. Ecol. 36 (6), 598–618. https://doi.org/10.1080/02757540.2020.1772244.

Chen, B., Liu, J., Qiu, J., Zhang, X., Wang, S., Liu, J., 2017. Spatio-temporal distribution and environmental risk of sedimentary heavy metals in the Yangtze River estuary and its adjacent areas. Mar. Pollut. Bull. 116, 469–478.

Daliri, M., Somma, R., Buccino, M., Troise, C., Molisso, F., De Natale, G., 2020-October. Numerical analysis of arsenic concentration in the marine sediments of bagnoli bay. In: Proceedings of the International Offshore and Polar Engineering Conference Volume, pp. 554–560.

Damiani, V., Baudo, R., De Rosa, S., De Simone, R., Ferretti, O., Izzo, G., Serena, F., 1987. A case study: bay of Pozzuoli (Gulf of Naples, Italy). Hydrobiology 149, 210–211.

Draper, N.R., Smith, H., 1981. Applied Regression Analysis, second ed. Wiley, New York.

Elliott, A.J., Barr, A.G., Kennan, D., 1997. Diffusion in Irish coastal waters. Estuarine. Coast. Shelf Sci. 44 (A), 15–23.

Fredsøe, J., Andersen, K.H., Sumer, B.M., 1999. Wave plus current over a ripple-covered bed. Coast Eng. 38, 177–221.

Gaeta, M.G., Samaras, A.G., Archetti, R., 2020. Numerical investigation of thermal discharge to coastal areas: a case study in South Italy. Environ. Model. Softw. 124, 104596 https://doi.org/10.1016/j.envsoft.2019.104596.

Giglioli, S., Colombo, L., Contestabile, P., Musco, L., Armiento, G., Somma, R., Vicinanza, D., Azzellino, A., 2020. Source apportionment assessment of marine sediment contamination in a post-industrial area (Bagnoli, Naples). Water 12, 2181, 2020.

Haghnazar, H., Hudson-Edwards, K.A., Kumar, V., Pourakbar, M., Mahdavianpour, M., Aghayani, E., 2021. Potentially toxic elements contamination in surface sediment and indigenous aquatic macrophytes of the Bahmanshir River, Iran: appraisal of phytoremediation capability. Chemosphere, 131446.

Hallermeier, R.J., 1981. A profile zonation for seasonal sand beaches from wave climate. Coast Eng. 4, 253–277.

Ibe, C.O., 2013. Elements of Random Walk and Diffusion Processes. Wiley.

ICRAM-SZN, 2005. Caratterizzazione ambientale dei fondali e degli arenili inclusi nella perimetrazione del sito di bonifica di Napoli Bagnoli-Coroglio. Relazione tecnica conclusiva, 2005 (BoI-Pr-CABA-relazione-02.04). In Italian.

Johnson, D., Pattiarachi, C., 2004. Transient rip currents and nearshore circulation on a swell-dominated beach. J. Geophys. Res. 109, C02026. https://doi.org/10.1029/2003JC001798, 2004.

Kullenberg, G., 1971. Vertical diffusion in shallow waters. Tellus 23 (2), 129–135. https://doi.org/10.3402/tellusa.v23i2.10372.

Larsen, B.E., Fuhrman, D.R., 2019. On the over-production of turbulence beneath surface waves in Reynolds-averaged Navier-Stokes models. J. Fluid Mech. 853, 419–460.

Li, Yanhong, Zhu, Yinian, Zhu, Zongqiang, Zhang, Xuehong, Wang, Dunqiu, Xie, Liwei, 2018. Fixed-bed column adsorption of Arsenic(V) by porous composite of magnetite/hematite/carbon with eucalyptus wood microstructure. J. Environ. Eng. Landsc. Manag. 26, 36–56.

Liu, Xun, Zeng, Biao, Guo, Lin, 2022. Arsenic (As) contamination in sediments from coastal areas of China. Mar. Pollut. Bull. 175, 113350.

Maillet, E., 1905. Essais d'hydraulique souterraine et fluviale. Librairie Sci., A. Hermann, Paris, p. 218.

Miller, M.C., Mc Cave, I.N., Komar, P.D., 1977. Threshold of sediment motion under unidirectional current. Sedimentology 24, 507–527.
Molisso, F., Caccavale, M., Capodanno, M., Di Gregorio, C., Gilardi, M., Guarino, A., Oliveri, E., Tamburrino, S., Sacchi N, M., 2020. ASedimentological analysis of marine deposits off the Bagnoli-Coroglio site of National interest (SNI), Pozzuoli (Napoli) bay. Chem. Ecol. 36 (6), 565–578. Jul 2020.
Morroni, L., d'Errico, G., Sacchi, M., Molisso, F., Armiento, S., et al., 2020. Integrated characterization and risk management of marine sediments: the case study of the industrialized Bagnoli area (Naples, Italy). Mar. Environ. Res. 160.
Nakamura, Y., Hayakawa, N., Nishimura, H., 1991. Vertical diffusivity in coastal seas. Coast. Eng. Jpn 34 (No. 1), 1991.
Nikuradse, J., 1932. Gesetzmässigkeiten der Turbulente Strömung in Glatten Rohren. Ver. Deut. Ing. Forschungsheft, p. 356.
Nishimura, H., Nakamura, Y., 1987. A new method of estimating vertical diffusion coefficient. Continent. Shelf Res. 7, 1245–1256.
Okubo, A., 1971. Oceanic diffusion diagrams. Deep-Sea Res. 18, 789–802, 1971.
Passaretti, S., Zheng, Y., Petitta, M., 2020. Redox dependent arsenic occurrence and partitioning in an industrial coastal aquifer: evidence from high spatial resolution characterization of groundwater and sediments. Water (Switzerland) Open Access ume 12 (Issue 10), 1–20. October 2020, Article number 2932.
Riddle, A.M., Lewis, R.E., 2000. Dispersion experiments in U.K. Coastal waters. Estuarine. Coast. Shelf Sci. 51, 243–254. https://doi.org/10.1006/ecss.2000.0661, 2000.
Romano, E., Bergamin, L., Ausili, A., Pierfranceschi, G., Maggi, C., Sesta, G., Gabellini, M., 2009. The impact of the Bagnoli industrial site (Naples, Italy) on sea-bottom environment. Chemical and textural features of sediments and the related response of benthic foraminifera. Mar. Pollut. Bull. 59, 245–256, 2009.
Romano, E., Bergamin, L., Celia Magno, M., Pierfranceschi, G., Ausili, A., 2018. Temporal changes of metal and trace element contamination in marine sediments due to a steel plant: the case study of Bagnoli (Naples, Italy). Appl. Geochem. 88, 85–94, 2018.
Samaras, A.G., Gaeta, M.G., Miquel, A.M., Archetti, R., 2016. High-resolution wave and hydrodynamics modelling in coastal areas: operational applications for coastal planning, decision support and assessment. Nat. Hazards Earth Syst. Sci. 16, 1499–1518. https://doi.org/10.5194/nhess-16-1499-2016.
Somma, R., Pooria, E., Troise, C., De Natale, G., Guarino, A., Cicchella, D., Albanese, S., 2021. The first application of compositional data analysis (CoDA) in a multivariate perspective for detection of pollution source in sea sediments: the Pozzuoli Bay (Italy) case study. Chemosphere 274, 2021.
Tamburrino, S., Passaro, S., Salvagio Manta, D., Quinci, E., Ausili, A., Romano, E., Sprovieri, M., 2020. Re-shaping the "original SIN": a need to re-think sediment management and policy by 635 introducing the "buffer zone" concept. In: Obhodas, J., Romano, E., Castellote, M., Heise, S. (Eds.), Special Issue "Sediments as a Dynamic Natural Resource – from Catchment to Open Sea", Journal of Soils and Sediments. https://doi.org/10.1007/s11368-019-02486-1.
Trifuoggi, M., Donadio, C., Mangoni, O., Ferrara, L., Bolinesi, F., Nastro, R.A., Stanislao, C., Toscanesi, M., 2017. Di Natale, G.; Arienzo, M. Distribution and enrichment of trace metals in surface marine sediments in the Gulf of Pozzuoli and off the coast of the brownfield metallurgical site of Ilva of Bagnoli (Campania, Italy). Mar. Pollut. Bull. 124, 502–511, 2017.
van Rijn, L.C., 2007. Unified view of sediment transport by currents and waves.I: initiation of motion, bed roughness, and bed-load transport. J. Hydraul. Eng. 133, 649–667, 2007.

Further reading

Damiani, V., et al., 1987. A case study: bay of Pozzuoli (Gulf of Naples, Italy). Hydrobiology.
Eckart, 1952. Eckart, C. 1952 The propagation of gravity waves from deep to shallow water. In Gravity Waves: (Proc. NBS Semicentennial Symp. on Gravity Waves, NBS, June 15–18, 1951), pp. 165–175. Washington: National Bureau of Standards. Washington: National Bureau of Standards., pp. 165–175